AIAA 2002-

AN EXPERIMENTAL INVESTIGATION OF THE FLOW STRUCTURE OF SUPERSONIC IMPINGING JETS

Brenda Henderson*, James Bridges**, Mark Wernet**
Kettering University, Mechanical Engineering Department

Abstract

An experimental investigation into the jet structure associated with sound production by a supersonic impinging jet is presented. Large plate impinging tones are investigated for a nozzle pressure ratio (NPR) of 4 and nozzle-to-plate spacings between 1 and 5 nozzle exit diameters, where NPR is equal to the ratio of the stagnation pressure to the pressure at the nozzle lip. Results from phase-locked shadowgraph and phase-averaged digital particle image velocimetry (DPIV) studies indicate that, during the oscillation cycle, the Mach disk oscillates axially, a well defined recirculation zone is created in the subsonic impingement region and moves toward the plate, and the compression and expansion regions in the outer supersonic flow move downstream. Sound appears to be generated in the wall jet at approximately 2.6R from the jet axis, where R is the nozzle exit radius. The oscillatory motion in the wall jet is the result of the periodic fluid motion in the near wall region.

A. Introduction

The impingement of a supersonic jet on a normal flat plate produces intense discrete frequency sound. Although the tones are known to be part of a feedback loop to the nozzle [see Powell[1] and Henderson and Powell[2]], the sound production mechanism is not well understood due to the complex nature of the flow. The jet is characterized by symmetrical, asymmetrical, and helical disturbances and oscillations of the shock waves and the near wall jet have been noted. Recirculation zones are sometimes observed for both steady and unsteady flow conditions. The purpose of this study is to understand better the connection between the production of discrete frequency sound and the periodic motion of the jet.

Supersonic impinging jets produce both small plate tones and large plate tones (see Powell[1] and Henderson and Powell[2]). Small plate tones typically appear for plate diameters less than, or equal to, two nozzle exit diameters and have frequency characteristics that are quite different from the large plate tones. Once the impinging plate diameter is greater than, or equal to, four nozzle exit diameters, only large plate tones are observed. Large plate tones are associated with asymmetrical, helical, and symmetrical jet disturbances for nozzle-pressure ratios (NPR) less than approximately 4, where NPR is equal to the ratio of the stagnation pressure to the pressure at the nozzle lip. As NPR increases to approximately 4, a single fundamental tone along with harmonics is usually present in the acoustic spectra and the tone is associated with symmetrical jet disturbances.

Unsteady shock motion is often associated with impinging jets but the important features of the motion appear to depend on the jet operating conditions and the size of the impingement plate. Golubkov et al.[3] reported a fluctuating compression shock, fluctuating plate pressures, and strong acoustic radiation when a small plate affected the central compression shock. Henderson and Powell[4] also noted large shock oscillations when tones were produced by jet impingement on a plate with the same diameter as the nozzle exit. When the jet impinges on a large plate, Semiletenko et al.[5] observed shock oscillations for operating conditions where only a single shock wave was present in the jet. When the nozzle-to-plate spacing increased to the point where two shock waves occurred in front of the plate, the oscillations ceased. Large oscillations of the standoff shock wave and the annular shock wave were noted by Henderson[6,7] and appeared to be connected to the production of tones. Despite the many observations of shock wave motion, the connection between this phenomenon and the production of discrete tones by large plate impingement is still not well understood.

Ginzburg et al.[8] was perhaps the first to note the connection between unsteady behavior in the jet and the occurrence of stagnation zones near the plate. Oscillations of the standoff shock wave were attributed to periodic fluid motion in the recirculation region behind the standoff shock wave. Ginzburg et al.[9] found that strong instability first occurred at the onset of recirculation in the impingement region. The numerical investigation of Iwamoto and Dekker[10] documented the motion of a toroidal vortex during the early stages of the impingement process. However, the connection between the presence of a recirculation region and the production of tones is unclear since recirculation zones have been reported for both steady and unsteady impinging jets [see Donaldson and Snedeker[11], Carling and Hunt[12], Gummer and Hunt[13], Kalghatgi and Hunt[14], and Gubanova et al.[15]].

The use of linear stability theory to explain small plate impinging tones has been reasonably successful. The one-dimensional instability model developed by Morch[16] provided for oscillations of the normal shock in front of the plate and acoustic waves traveling in the

subsonic flow between the plate and the shock wave. A strong resonance condition was not obtained from this analysis. However, when Kuo and Dowling[17] accounted for entropy changes, strong resonance occurred and the resulting resonance frequencies matched those measured for small plate impingement although the analysis did not restrict the diameter of the plate. The inability to explain the production of large plate tones was perhaps due to the lack of upstream forcing of the Mach disk.

The development of a sound production model for large plate impinging tones requires a better understanding of the impingement and near wall regions of the jet. The effect of shock wave oscillations and the occurrence of stagnation zones on the production of tones are investigated in this study.

B. Experimental Apparatus

The experiments were performed with the Small Hot Jet Aeroacoustics Rig (SHJAR) at NASA Glenn Research Center shown in Fig. 1. Air entered the rig through a 102 mm diameter line at 1034 kPa. Two low noise control valves and a vernier valve were used to regulate NPR. The flow passed through two 90° elbows then entered a 356 mm diameter plenum chamber located 3.05 m above the facility floor. The plenum chamber was instrumented with total pressure probes that were used to monitor NPR. An ASME bellmouth contraction followed the plenum chamber and passed the flow to a 152 mm diameter pipe containing three flow straightening screens. The flow exhausted through a convergent nozzle with a cubic contour and an exit diameter of 25.4 mm. The external contour of the nozzle was a 30° cone and the nozzle lip thickness was 12.7 mm. A 533 mm x 610 mm aluminum plate was placed normal to, and traversed along, the jet axis.

The SHJAR is located in the Aeroacoustic Propulsion Laboratory (AAPL) at NASA Glenn Research Center. The laboratory is a 20 m radius, geodesic dome with fiberglass wool acoustic wedges on the walls and approximately half of the floor area.

The shadowgraph system was located on the traversing mechanism used for the plate. A Photonics Analysis Pal Flash produced light with approximately a 1μsec spark duration. The light was focused onto a pinhole located at the focal point of a 508 mm diameter spherical mirror with a 2.54 m focal length. The parallel rays from the spherical mirror passed through the test section and were intercepted by another 508 mm diameter spherical mirror with a 2.54 m focal length. The shadowgraph images were focused onto a Kodak DX1 digital camera. A Bruel and Kajer _" type 4135 was placed in the far field and used to trigger the phase-locked shadowgraph photographs. The microphone signal was first filtered then recorded on a Yokogawa type DL708E digital oscilloscope. The trigger output signal from the oscilloscope was time delayed using a Model DG 535 Stanford Research Digital Delay Generator then used to trigger the light source at the desired locations in the oscillation cycle, but not the same cycle.

The general configuration used for the digital particle image velocimetry (DPIV) studies is shown in Fig. 1. A Continuum PIV-Surlite III, 400 mJ, Nd:Yag, dual head laser with a maximum repetition rate of 10 Hz was used to produce light pulses with a 1.2 μsec inter-frame time delay. A light sheet was formed with one cylindrical and one spherical lens resulting in a light sheet thickness of approximately 0.2 mm. Images were recorded on a Redlake ES 4.0 digital camera with a 2048 x 2048 pixel CCD array. For nozzle-to-plate spacings less than 75 mm, an 80 mm field of view was used. For larger nozzle-to-plate spacings, the field of view was 136 mm.

The jet was seeded with 0.6 μm olive oil droplets using two TSI model 9306 Six-jet Atomizers. The ambient air was seeded with 0.2 – 0.3 μm smoke particles using a Vicount 5000 smoke generator. A typical image acquired in the PIV studies is shown in Fig. 2.

For phase averaged PIV studies, the filtered microphone signal and the q-switch signal from the lasers were recorded on an RC Electronics Datamax data acquisition unit. The vector plots corresponding to images acquired at the same phase location were averaged from a total of 800 image pairs acquired at each unsteady operating condition. Between 20 and 60 vector plots were averaged at each phase location.

The collected DPIV images were processed using PIVPROC (see Wernet[18]), a NASA Glenn Research Center (GRC) developed code. The correlation based processing allows subregion image shifting and multi-pass correlation to improve the spatial resolution of the resultant velocity vector maps. In the multi-pass correlation processing, a first pass subregion size of 64 x 64 pixels is used with a 50% overlap. The second pass uses a subregion size of 32 x 32 pixels, again with a 50% overlap. The resulting spatial resolutions of the velocity vector grids are 0.6 mm and 1.06 mm for the 80 mm and the 133 mm field of views, respectively.

C. The Creation of Stagnation Zones

The creation of recirculation zones near the plate was perhaps first explained by Ginzburg et al.[8]. A schematic of the impingement flow is shown in Fig. 3.

A shear layer (region 3 in Fig. 3) forms between the subsonic flow in the central region of the jet behind the Mach disk (region 1 in Fig. 3) and the supersonic flow in the peripheral regions of the jet behind the oblique shock (region 2 Fig. 3). The total pressure lost by the flow passing through the Mach disk is greater than that lost by the flow behind the oblique shock. The difference in total pressure loss results in a low-pressure at the center of the plate and a pressure maximum in the peripheral regions of the jet. Part of the flow passing through the Mach disk is drawn into the shear layer and leaves the central domain upstream of region 4. Near the plate, a portion of the flow cannot overcome the peripheral pressure maximum and forms a recirculation zone near the plate (region 5 in Fig. 3).

The formation of an annular shock wave in the peripheral regions of the jet (region 7 in Fig. 3) was discussed by Henderson and Powell[2,4] and Henderson[6,7]. An expansion fan occurs at the intersection of the jet boundary and oblique shock (region 6 in Fig. 3). The expansion waves reflect from the constant pressure boundary between the subsonic flow and supersonic flow as compression waves that merge to form an annular shock wave. Carling and Hunt[12] found that the pattern of compression and expansion continues to persist well into the wall jet for several jet radii. However, when the waves reach the plate, the pattern is somewhat altered by in-phase reflection at the plate surface.

D. Experimental Results

D.1 Acoustic Measurements

A typical acoustic spectrum produced by a moderately underexpanded impinging jet is shown in Fig 4. A very intense discrete frequency tone is produced at the fundamental frequency along with multiple harmonics. As shown in the figure, the fundamental tone is often at least 20 dB above the broadband noise.

A plot of the normalized acoustic wavelength versus the normalized nozzle-to-plate spacing is shown in Fig. 5. The acoustic wavelength is given by λ and the nozzle exit diameter and the nozzle-to-plate spacing are given by d and h, respectively. The tones falling along the L1 line have been shown[11] previously to be associated with symmetrical jet disturbances. The first 'zone of silence' occurs at approximately h/d = 2.70 and the second 'zone of silence' begins at approximately h/d = 3.8. Also indicated in the figure are the nozzle-to-plate locations where the phase averaged DPIV studies and the phase locked shadowgraph studies were performed.

D.2 Phase-locked Shadowgraph Studies

Phase-locked shadowgraph photographs taken at the operating conditions indicated in Fig. 5 are shown in Fig. 6. The location of each photograph in the oscillation cycle, but not the same cycle, is referenced to the location corresponding to the photograph in Fig. 6 (a). The time, t, has been normalized by the period, T.

In Fig. 6 (a), a Mach disk intersecting a conical shock wave and an annular shock wave are present in the jet. As time progresses [see Figs. 6 (b) and (c)], the annular shock wave moves downstream and waves in the central region of the jet behind the Mach disk propagate toward the plate. At t/T = 0.6 [Fig. 6 (d)], the annular shock wave weakens significantly and nearly disappears. Toward the end of the oscillation cycle at t/T = 0.8, both the annular shock wave and the waves in the central region of the jet disappear [see Fig. 6 (e)].

The sound waves propagating upstream in the ambient flow appear to originate in the near wall region of the jet. A periodic thickening of the near wall region as the annular shock wave propagates downstream is also evident in the photographs. However, the light rays at this location must pass through the entire wall jet so the appearance of the flow along and near the jet centerline may be somewhat distorted.

The linear stability analysis of Kuo and Dowling[17] indicates that a strong resonant condition exists in the region between an oscillating normal shock wave and an impinging plate. Oscillations of the shock give rise to acoustic and entropy waves traveling in the region behind the shock. The deceleration of the entropy waves as the plate is approached results in additional acoustic waves. The subsequent interaction of the reflected waves with the shock causes the shock oscillations to persist. However, only small plate tones are described by the linear analysis, perhaps due to the lack of interaction of the shock wave with waves generated at the nozzle lip. The waves observed in the central region of the jet in Fig. 6 are most likely related to the acoustic and entropy waves described by Kuo and Dowling, but the feedback cycle must involve disturbances generated at the nozzle as indicated by the studies of Henderson and Powell[2].

The shadowgraph photograph in Fig. 7 was taken at a non-tone producing operating condition. Due to the larger nozzle-to-plate spacing, a second (dome-shaped) shock occurs in the jet and the annular shock wave

resides close to the plate. The elimination of instability by the addition of a second shock wave is consistent with the observations made by Semiletenko et al.[12] However, as the nozzle-to-plate spacing increases, discrete tones will reappear as indicated by the acoustic data in Fig. 5.

D.3 Phase Averaged DPIV studies

Vector contour plots obtained from the phase-averaged DPIV studies are shown in Fig. 8. Figure 8 (a) has been arbitrarily chosen as the beginning of the oscillation cycle and is located at approximately the same point in the oscillations cycle as the shadowgraph photograph in Fig. 6 (a).

Although particle lag is expected to introduce errors in the velocity measurements behind the shock, the purpose of the studies was to identify the major flow features in the oscillation cycle and particle lag is not expected to prevent the identification of these features. Studies conducted at other nozzle-to-plate spacings where L1 tones are produced indicate that the flow oscillation cycle is quite similar for all nozzle-to-plate spacings in the range of $1.59 \leq h/d \leq 2.34$ and is well represented by the plots in Fig. 8.

The plots in Fig. 8 show that the flow in the impingement region is divided into a subsonic region behind the Mach disk, and a supersonic region behind the conical section of the first shock wave. The outer supersonic flow has alternating regions of expansion and compression as described in Section C. The compression waves most likely merge into the annular shock wave observed in the shadowgraph photographs.

At the beginning of the oscillation cycle [see Fig. 8 (a)], a recirculation zone resides in the subsonic flow close to the plate. A contact surface, region 4 in Figs. 3 and 8, develops between the recirculating flow and the flow upstream which is pushed outward toward the shear layer. As time progresses, the Mach disk moves downstream [see Fig. 8 (b)] and a new contact surface develops behind the Mach disk while the previous contact surface disappears. A new recirculation zone begins to develop behind the new contact surface and the recirculation zone near the plate moves outward. By $t/T = 0.0334$ [see Fig. 8 (c)], the recirculation zone near the plate collapses and the contact surface along with the upstream recirculation zone continue to move downstream for the remainder of the oscillation cycle. The Mach disk begins to move upstream at $t/T = 0.52$ [see Fig. 5 (d)].

As the recirculation zones and associated contact surface move downstream, the shear layer between the inner subsonic flow and the outer supersonic flow distorts. In the outer supersonic flow, the alternating regions of compression and expansion move toward the plate and the two expansion regions merge in Fig. 8 (d) at $t/T = 0.502$, close to the location in the oscillation cycle where the annular shock begins to disappear in the shadowgraph photographs. The motion of the compression and expansion regions is most likely associated with the motion of the annular shock observed in the shadowgraph photographs.

Pronounced oscillations occur in the wall jet at approximately 2.6 jet radii from the jet centerline (2.6R in Figs. 6 and 8) and are the result of the motion of recirculation zones in the inner subsonic flow and compression and expansion regions in the outer flow. At this location in the wall jet, the flow velocity reaches a minimum at $t/T = 0.334$ [see Fig. 8 (c)] and the entrained velocity in the adjacent flow is directed into the wall jet region. At $t/T = 0.836$ [see Fig. 8 (e)], the entrained velocity is pushed outward and becomes tangent to the wall. The sound is most likely produced in the wall jet with fluctuations of the jet boundary acting as a simple source distributed over an annulus centered at this location.

The average vector plot obtained from DPIV studies conducted at a non-tone producing operating condition is shown in Fig. 9. A second (dome-shaped) shock wave stands in front of the plate due to the larger nozzle-to-plate spacing. The flow in the central region of the jet behind the standoff shock wave is at subsonic speeds and the flow in the peripheral regions of the jet is at supersonic speeds. A stagnation region occurs in the subsonic flow close to the plate. Evidently the presence of a recirculation region does not guarantee instability and the production of discrete tones.

E. The Feedback Loop

The results of phase averaged DPIV studies conducted for a range of nozzle-to-plate spacings indicate that an oscillating recirculation zone is always present in the impingement region when L1 tones are produced. The recirculation zone is the result of a greater loss in stagnation pressure behind the Mach disk than in the peripheral regions of the jet behind the oblique shock. As the Mach disk experiences small oscillations, pressure waves propagate in the region between the standoff shock wave and the plate and cause the recirculation zones to move. The pressure waves are most likely associated with the acoustic and entropy waves described by Kuo and Dowling[17]. A contact surface occurs upstream of the recirculation zones causing the upstream flow to be directed outward toward the shear layer and sonic line. A wave is

produced in the supersonic peripheral flow due to distortions of the sonic line and induced velocity from the moving recirculation zones. The wave in the outer supersonic flow results in the motion (and subsequent collapse) of the annular standoff shock wave.

As the recirculation regions in the inner flow and compression and expansion regions in the outer flow oscillate, the wall jet oscillates near 2.6R from the jet centerline and sound is produced. The sound propagates upstream and produces disturbances that propagate downstream and cause oscillations of the Mach disk, thus closing the feedback loop.

Subtracted velocity fields, shown in Fig. 11 and schematically in Fig. 10, were obtained at each point in the oscillation cycle for the purpose of better understanding the feedback cycle. The phase-averaged subtracted field was obtained by subtracting each of the phase-averaged velocity fields in Fig. 8 from the average velocity field obtained from 800 image pairs.

In Fig. 11, regions of unsteady rotating and counter-rotating velocity components can be identified in the flow behind the Mach disk (labeled regions 1 and 2 in Figs. 10 and 11). The regions move downstream toward the plate and collapse at approximately t/T = 0.502 (clockwise velocity component) and 0.836 (counterclockwise velocity component) near the wall at a radius of approximately 1.6R from the jet centerline. The unsteady component of the velocity in the wall jet at a radius of 2.6R from the jet centerline is directed outward for t/T < 0.502 and inward for t/T > 0.502. The reversal of the unsteady flow in the wall jet results in the oscillations observed in Fig. 8. Unsteady plate pressure measurements conducted by Henderson[6,7] indicate that a secondary pressure maximum occurs at approximately 1.6R for a nozzle-to-plate spacing of h/d = 1.74. The secondary pressure maximum is most likely associated with the changes in the unsteady flow noted above.

The application of Powell's[19] feedback criterion to impinging jet tones [see Powell[1] and Henderson and Powell[2]] can be refined with the detailed description of the oscillation cycle obtained from the DPIV studies. The criterion states that the required time for a particular phase of the disturbance to travel through the entire feedback loop must be equal to $\frac{N+p}{f}$, where N is an integer and p is a non-integer. The non-integer is necessary to account for the fact that the phases of the disturbance and sound wave may not be identical at the sound source and nozzle exit. The feedback criterion is given by

$$\frac{(N+p)}{f} = \int_0^{h_1} \frac{(dh)}{u_{1con}} + \int_{h_1}^{h_2} \frac{(dh)}{u_{2con}} + \int_s^0 \frac{(dh)}{c}, \qquad (1)$$

where h_1 is the distance between the nozzle and the Mach disk (see Fig. 11), h_2 is the distance traveled by the unsteady rotational components in the impingement and near wall regions, and s is the distance between the sound source in the near wall region and the nozzle exit. The quantities u_{1con} and u_{2con} are the convection velocities of the disturbances before and after the Mach disk, respectively. The speed of the sound in the ambient flow, c, is reasonably constant so integration is not required for the last term.

A plot of the displacement of the unsteady rotating flow obtained from the subtracted velocity plots in Fig. 10 is shown in Fig. 12. The rotational component disappears at t/T = 2 and the unsteady flow in the wall jet reverses direction. The plot indicates that the convection velocity, u_{2con}, is reasonably constant so that the second integral on the right hand side of Eq. (1) may be replaced by $\frac{\Delta x_{max}}{u_{1con} d}$, where Δx_{max} is the maximum displacement at t/T = 2 and u_{2con} is determined from the slope of the line in Fig. 12.

The first integral on the right hand side of Eq. (1) can usually be replaced with the ratio of the distance traveled by the jet disturbances divided by an appropriate average convection velocity determined from schlieren photographs or subtracted vector fields. It was not possible to locate the jet disturbances upstream of the Mach disk from the data available in the present study possibly due to the small nozzle-to-plate spacing. However, Powell[1] and the photographs in Henderson and Powell[2] indicate that the average convection Mach number given by $\overline{M}_{2con} = \frac{\overline{u}_{con1}}{c}$ is equal to 0.7 – 0.75, where an overbar indicates an average quantity. The distance between the nozzle and Mach disk, h_1, can be determined from Henderson[6,7] for a range of nozzle-to-plate spacings and NPR.

Equation (1) may be reformatted to yield

$$(N+p)\left[(0.7)\frac{h}{d}\right] = \frac{h_1/d}{\overline{M}_{1con}} + \frac{h_2/d}{\overline{M}_{2con}} + \frac{s}{d}, \qquad (2)$$

after multiplying Eq. (1) by the speed of sound c, dividing by the nozzle exit diameter d, and setting λ/d equal to 0.69h/d as indicated by the data in Fig. 5. The quantity $\overline{M}_{2con}$ is equal to $\frac{\overline{u}_{2con}}{c}$.

Using experimentally determined values for the quantities in Eq. (2) at h/d = 2.02, N is found to be equal to 4 and p is equal to approximately 0.4. Krothapalli et al.[20] found that p was equal to –0.4 for the ideally expanded supersonic impinging jet. However, a standoff shock wave was usually not present for the ideally expanded jet so the feedback loop is presumably quite different.

F. Conclusions

When large-plate, L1 tones are produced by a supersonic impinging jet, small oscillations of the Mach disk cause motion of the recirculation zone in the impingement region and motion of the compression and expansion regions in the outer supersonic flow. The resulting flow near the plate oscillates and produces well-defined oscillations of the wall jet at a radius of approximately 2.6R from the jet centerline. The wall jet boundary in this region appears to act as a simple source to produce sound. The application of Powell's[19] feedback criterion shows that the value of N+p is equal to nearly 4.4.

Acknowledgements

The authors thank Kenneth Weiland, Wentworth John, and Garret Clayo of NASA GRC for their assistance throughout this project.

References

1. A. Powell, "The sound-producing oscillations of round underexpanded jets impinging on normal plates," J. Acoust. Soc. Am. **83**, 515-533 (1988).
2. B. Henderson and A. Powell, "Experiments concerning tones produced by an axisymmetric choked jet impinging on a flat plate," **168(2)**, 307-326 (1993).
3. A. G. Golubkov, B. K. Koz'menko, V. A. Ostapenko, and A. V. Solotchin, "On the interaction of an underexpanded supersonic jet with a finite flat baffle," Fluid Mechanics-Soviet Research **3**, 96-102 (1974).
4. B. Henderson, and A. Powell, "Sound-producing mechanisms of the axisymmetric choked jet impinging on small plates: the production of primary tones," J. Acoust. Soc. Am. **99**, 153-162 (1996).
5. B. G. Semiletenko, B. N. Sobkolov, and V. N. Uskov, "Features of unstable interaction between a supersonic jet and infinite baffle," Fluid Mechanics-Soviet Research **3(1)**, 90-95 (1974).
6. B. Henderson, "An experimental investigation into the sound producing characteristics of supersonic impinging jets," 7th AIAA/CEAS Aeroacoustics Conference, Maastricht, The Netherlands, paper no. AIAA 2001-2145.
7. Henderson – 2002 ASA article
8. I. P.Ginzburg, B. G. Semiletenko, V. S. Terpigor'ev, and V. N. Uskov, "Some singularities of supersonic jet interaction with a plane obstacle," J. Engineering Physics 19, 1081-1084 (1973). (Translated from Inzhenerno-Fizicheskii Zhurnal 19(3), 412-417 (1970)).
9. I. P. Ginburg, V. N. Semiletenko, and V. N. Uskov, "Experimental study of underexpanded jets impinging normally on a plane baffle," Fluid Mechanics-Soviet Research **4(3)**, 93-105 (1975).
10. J. Iwamoto and B. E. L. Deckker, "Development of flow field when a symmetrical underexpanded sonic jet impinges on a flat plate, J. Fluid Mech. **113**, 299-313 (1981).
11. C. D. Donaldson and R. S. Snedeker, "A study of free jet impingement. Part 1. Mean properties of free and impinging jets," J. Fluid Mech. **45**, 281-319 (1971).
12. J. C. Carling and B. L. Hunt, "The near wall jet of a normally impinging, uniform, axisymmetric, supersonic jet," J. Fluid Mech. **66**, 159-176 (1974).
13. J. H. Gummer and B. L. Hunt, "The impingement of non-uniform, axisymmetric supersonic jets on a perpendicular flat plate," Israel J. Tech. **12**, 221-235 (1974).
14. G. T. Hunt and B. L. Hunt, "The occurrence of stagnation bubbles in supersonic jet impingement flows, Aero. Quart. **27**, 169-185 (1976).
15. O. I. Gubanova, V. V. Lunev, and L. N. Plastinina, "The central breakaway zone with interaction between a supersonic underexpanded jet and a barrier," Fluid Dynamics **6**, 298-302 (1973). (Translated from Izvestiya Akademii Nauk SSSR, Mekhanika Zhidkosti I Gaza **2**, 135-138 (1971)).
16. K. A. Morch, "A theory for the mode of operation of the Hartmann air jet Generator," J. Fluid Mech. **20**, 141-159 (1964).
17. C. Kuo and A. P. Dowling, "Oscillations of a moderately underexpanded choked jet impinging upon a flat plate," J. Fluid Mech. **315**, 267-291 (1996).
18. M. P. Wernet, "Fuzzy logic digital PIV processing software," Proceedings of the 11th International Congress on Instrumentation for Aerospace Simulation Facilities (ICIASF), Toulouse, France, (1999).
19. A. Powell, "On edge tones and associated phenomena," Acustica **3**, 233-243 (1953).
20. A. Krothapalli, E. Rajkuperan, F. Alvi, and L. Lourenco, "Flow field and noise characteristics of a supersonic impinging jet," J. Fluid Mech. **392**, 155-181 (1999).

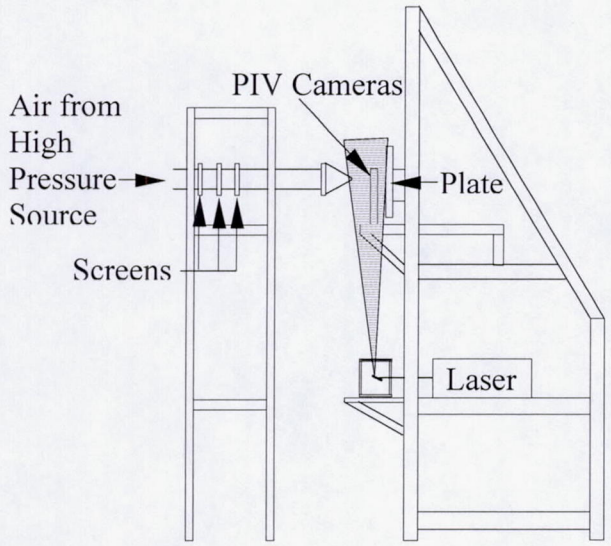

Figure 1. Apparatus used in impinging jet experiments.

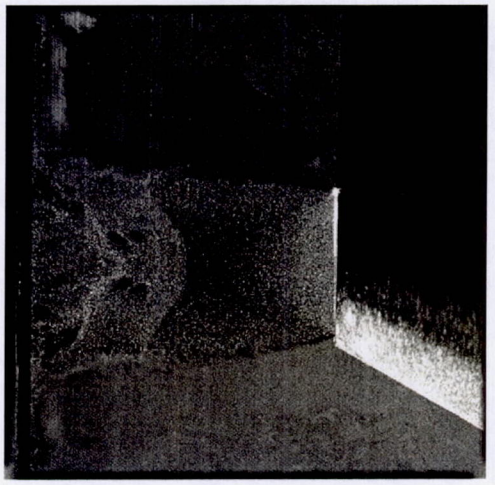

Figure 2. A typical image acquired in the DPIV studies.

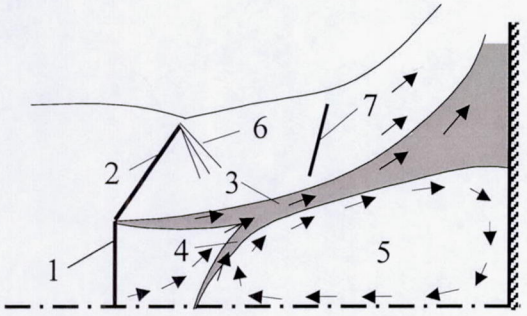

Figure 3. A schematic of the impingement region of the jet.

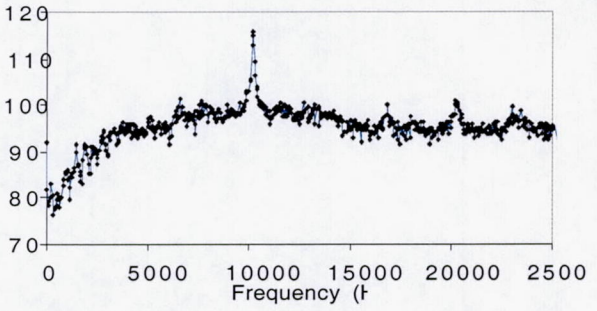

Figure 4. The power spectrum acquired at NPR = 4.03 and h/d = 2.02.

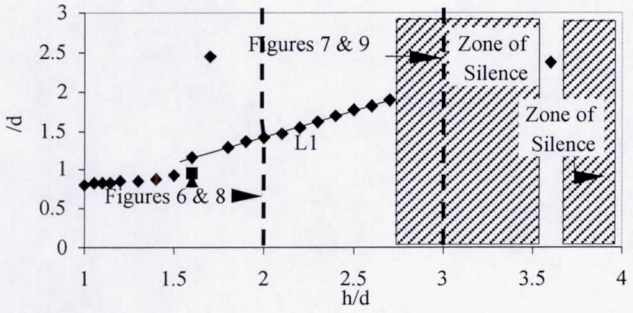

Figure 5. Normalized acoustic data for a range of nozzle-to-plate spacings.

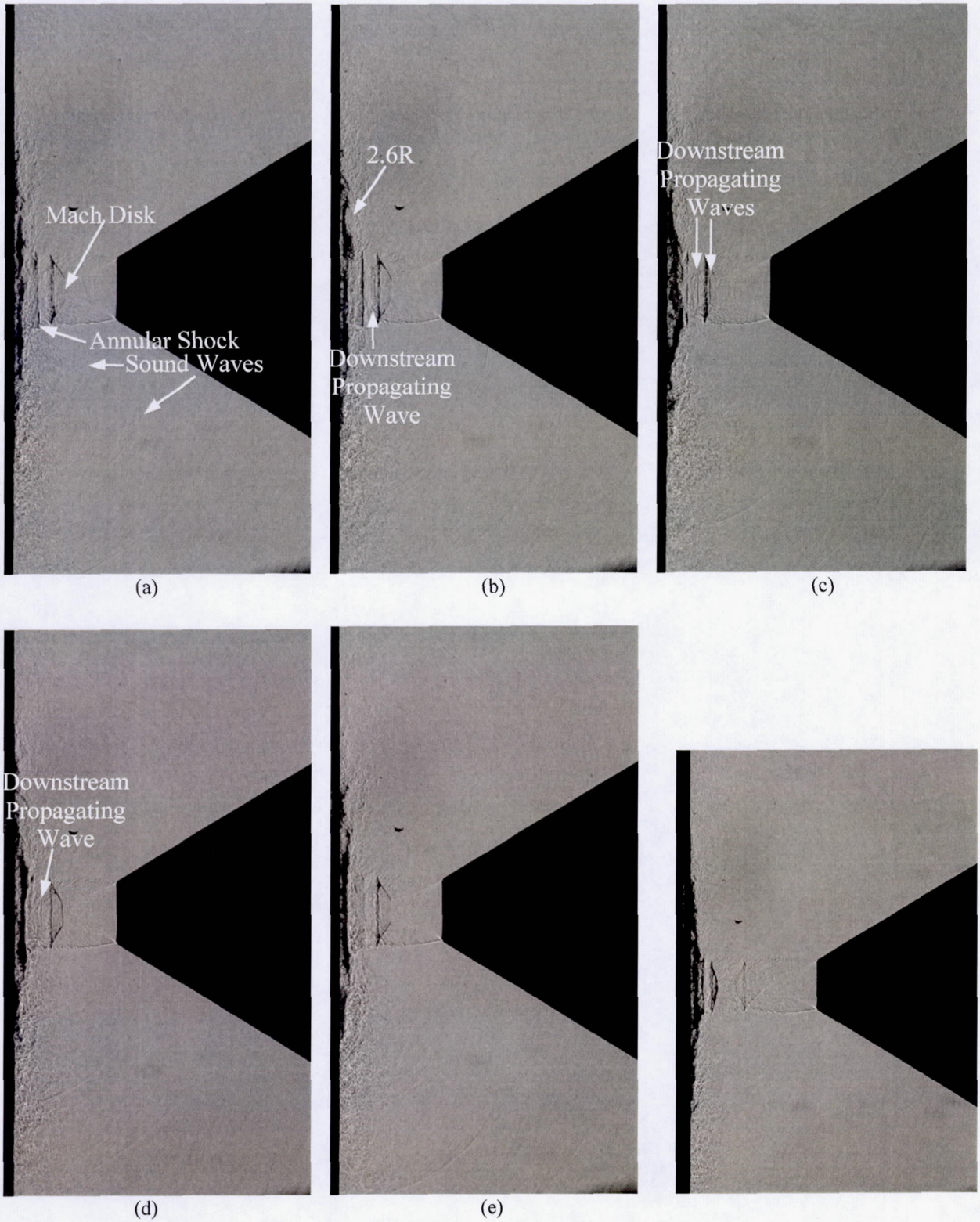

Figure 6. Phase-locked shadowgraph photographs taken at NPR = 4.03, h/d = 2.02, and (a) t/T = 0, (b) t/T = 0.2, (c) t/T = 0.4, (d) t/T = 0.6, and (e) t/T = 0.8.

Figure 7. Shadowgraph photograph taken at NPR = 4.03 and h/d = 3.00.

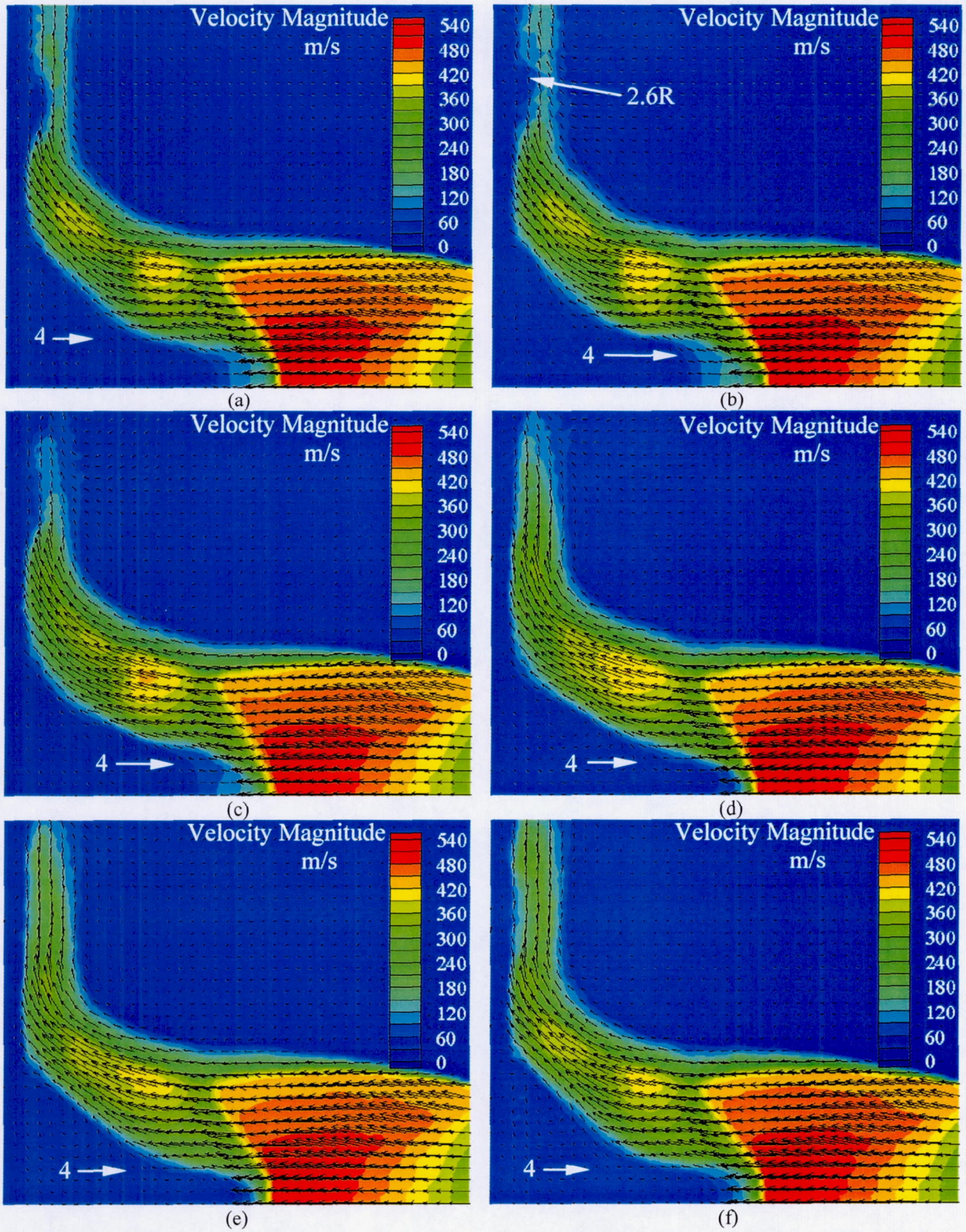

Figure 8. Phase-averaged vector and contour plots obtained from DPIV studies conducted at NPR = 4.03, h/d = 2.02 and (a) t/T = 0, (b) t/T = 0.167, (c) t/T = 0.334, (d) t/T = 0.502, (e) t/T = 0.669, and (e) t/T = 0.836.

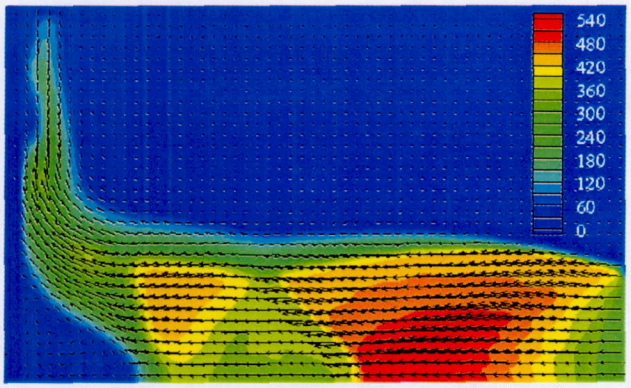

Figure 9. The average velocity vector plot obtained from DPIV studies conducted at NPR = 4.03 and h/d = 3.00.

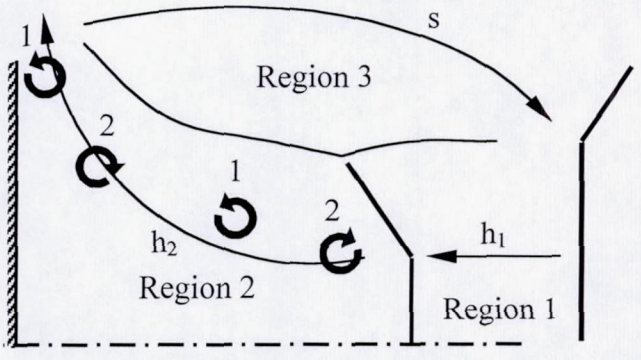

Figure 10. A schematic of the flow field shown in Fig. 11.

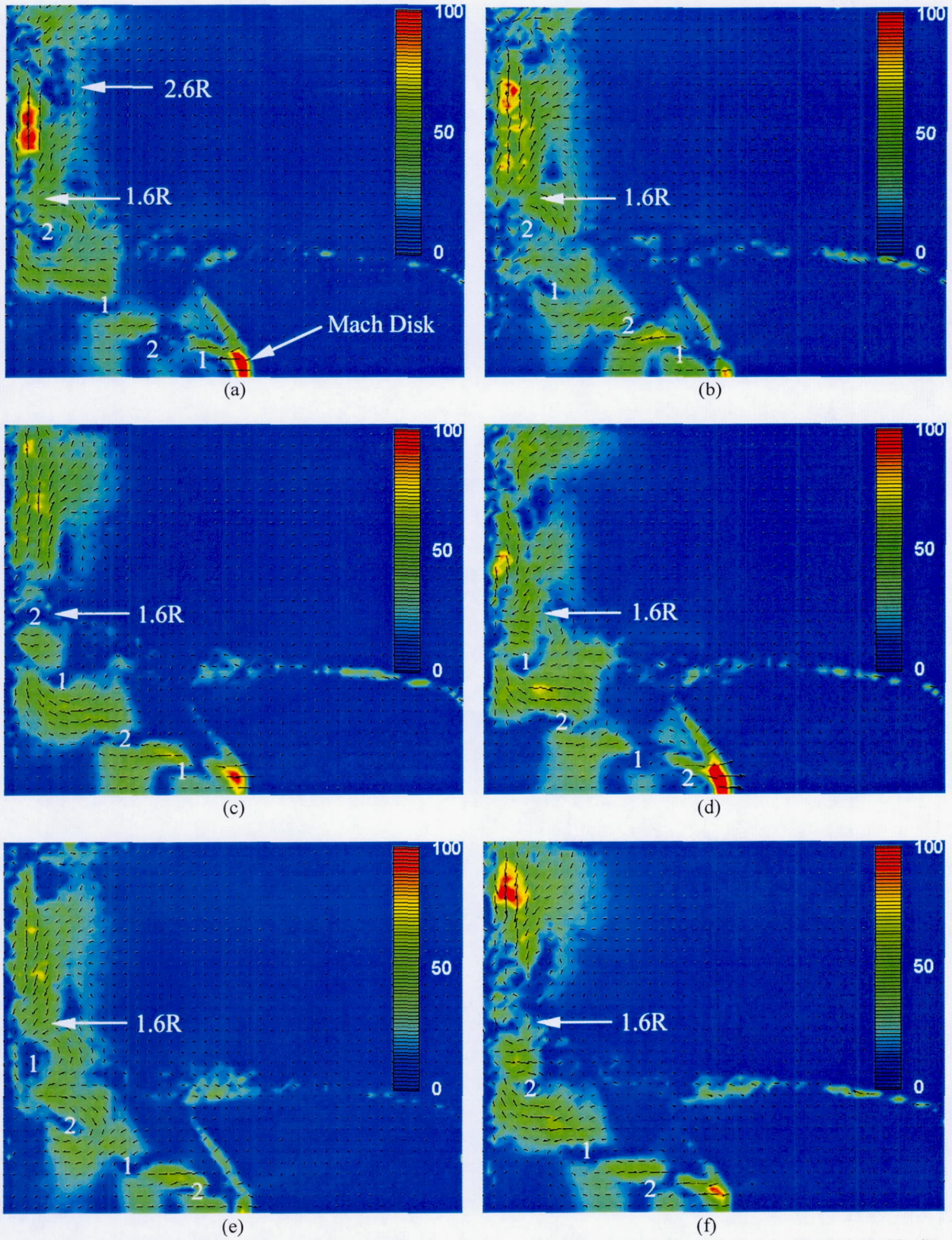

Figure 11. Subtracted vector plots for NPR = 4.03, h/d = 2.02 and (a) t/T = 0, (b) t/T = 0.167, (c) t/T = 0.334, (d) t/T = 0.502, (e) t/T = 0.669, and (e) t/T = 0.836.

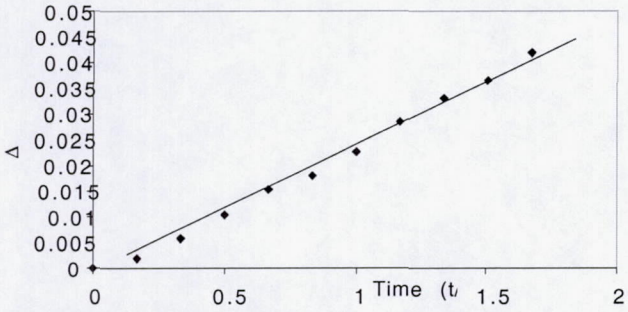

Figure 12. The displacement of the unsteady rotational velocity component in Fig. 11 (region1).